Characteristics of Prototype Silicon Sensors for Run2b

K. Hara and Y. Takei

University of Tsukuba, Tsukuba, Ibaraki, Japan

Abstract

We describe the characteristics of Hamamatsu silicon sensors prototyped for Run2b silicon detector. In the prototype program, 60 axial and 53 stereo sensors have been fabricated. The performance results including those after neutron irradiation are presented, which are superior in all aspects and fulfill our specifications.

1. Introduction

The CDF collaboration is building a new silicon tracker system for Tevatron collider Run2b, replacing the present L00 and SVXII detectors. The new silicon system will be a six-layer device located between 2.1 cm and 16 cm radius, consisting of ~2300 single sided silicon sensors. The planned silicon detector is expected to become operational in early 2005.

The specifications of silicon sensors are described in detail in an accompanying note. Table 1 summarizes the main specification:

- Operational voltage should exceed beyond 500V
- Full depletion voltage should be in the range from 120 to 250V
- Dead channel fraction should be less than 1%
- Sensors should be uniform in coupling capacitance, bias resistance, interstrip resistance, and other electrical properties

Table 1: Main sensor specifications

Specifications:	**Inner Axial**	**Outer Axial/Small Stereo**
Wafer	Orientation: <100> Thickness: 320±15μm Warp: less than 130μm	
Full depletion voltage	120<Vdep<250V	
Leakage current	<50nA/cm^2 at RT and at 500V	
Junction breakdown	>500V	
Implant width	7μm	8μm
Al width	1-3 μm overhanging metal	2-3 μm overhanging metal
Coupling capacitance	>90pF	
Coupling capacitor breakdown	>100V	
Interstrip capacitance	<1.2pF/cm	
Polysilicon bias resistor	1.5±0.5 MΩ	
Defective strips	<1%	
Readout strip pitch	50 μm	75μm /80μm
Intermediate strip		yes
Interstrip resistance	>1GΩ even after irradiation	

2. Production of Prototype Sensors

The prototype outer axial and stereo sensors were fabricated by Hamamatsu Photonics (HPK). We received 60 and 53 pieces for axial and stereo sensors, respectively. While the production of axial sensors completed as scheduled, the delivery of stereo sensors was delayed by 2-3 weeks since one component in the process line was broken and replaced. Therefore, the stereo wafers were removed from the line, which created small scratches on the sensor surfaces. The stereo sensor yield was thus not as high as the axial sensors.

3. Electrical Characteristics

We have evaluated those electrical characteristics listed in Table 1 using a computer controlled probe station. The measurement procedures are described in detail in the accompanying note. In this note, we summarize the measurement results on the following items:

(1) I-V curve: Total leakage current is measured as a function of bias voltage up to 1000V at a step of 10V.
(2) Stability of I-V curve: I-V curves are measured every 30 min at least for 10 times. The bias voltage between I-V measurements is kept at 200 V.
(3) C-V curve: Total capacitance is measured as a function of bias voltage. The C-V curve is used to extract the full depletion voltage.
(4) AC scan: Coupling capacitance, implant + bias resistance, and oxide punch-through at 100V are measured for each readout strip.
(5) DC scan: The leak current of individual strip is measured for sensors with large total leakage. The bias is set above the micro-discharge onset voltage.
(6) Interstrip isolation: The interstrip resistance is measured applying voltages (-1 to +1V) to the neighboring intermediate DC pads and measuring the current emerging from the readout DC pad.
(7) Interstrip capacitance: The capacitance between the neighboring AC pads is measured with others at floating.
(8) Long-term stability: The leakage current is read out periodically while keeping the bias voltage at 500V.

In addition to the above, diagnostic measurements were carried out to identify the problems. For example, when leaky intermediate strips are reported by HPK, we scanned intermediate strips for strip leakage current. Note that intermediate strips are not tested in usual scans. Should HPK failed to identify leaky intermediate strips, DC scan would be performed on readout strips and then on intermediate strips if readout strip leakage can not explain the large total leakage current. We can safely ignore somewhat leaky intermediate strips as far as the total leakage current is manageable. Also, when the implant strip is reported to be open by HPK, we first look at AC scan data (the coupling capacitance and series resistance are smaller if implant is open), then the strip is carefully inspected under microscope. If there is no clear open found, we measure the resistance between the DC pad and the bias-ring (very large if the intermediate implant is open), and other characteristics. We always inspect carefully under microscope when any irregularities are recognized.

3.1 I-V curves

Figures 1a and 1b show I-V curves of 60 axial and 53 stereo sensors. Most of the sensors do not show significant micro-discharge up to 1000V we measured. Exceptions are #010 and #048

stereo sensors, which showed micro-discharge at voltages above 300V-450V. As described in 3.5, single leaky strip contributes to the micro-discharge for both sensors. The I-V curve of these sensors tend to become moderate as bias is kept applied, as described in 3.2. We set our leakage current requirement less than 2 μA at 500V so that no single readout strip has significant leakage current, ~1μA, which degrades the noise performance. In this view, all the sensors fulfill our specification (#010 stereo is just on the boundary). Actually substantial fraction of ISL sensors had leakage current close to even a relaxed specification. The present prototypes are roughly one order better in the leakage current. We should, though, avoid using these two sensors as far as the

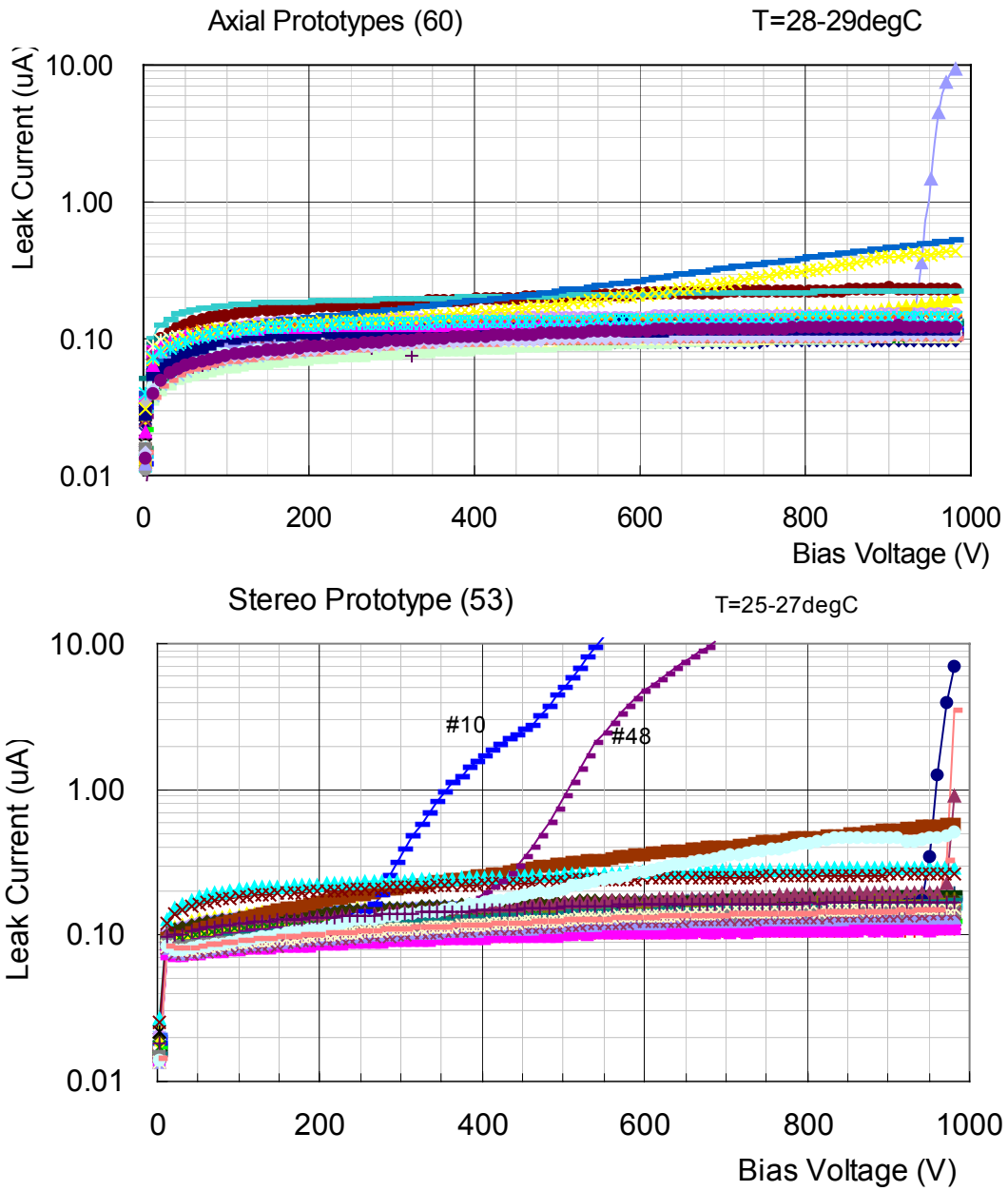

Fig. 1a (top) I-V curves of 60 axial sensors.
Fig. 1b (above) I-V curves of 53 stereo sensors.

delivery goes as scheduled and we receive sensors with similar performance.

3.2 Stability of I-V curves

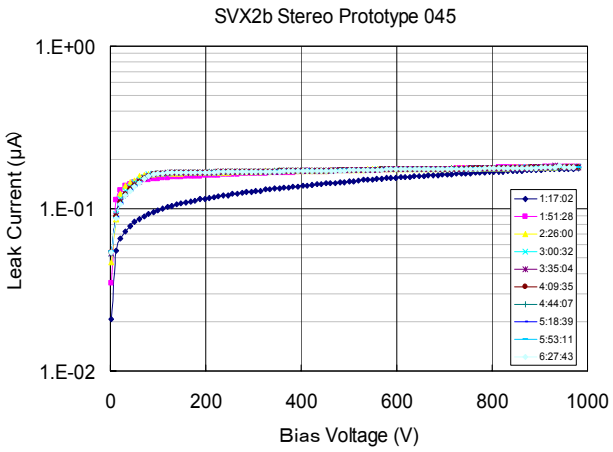

Fig. 2a Typical I-V stability of sensor #045 (stereo).

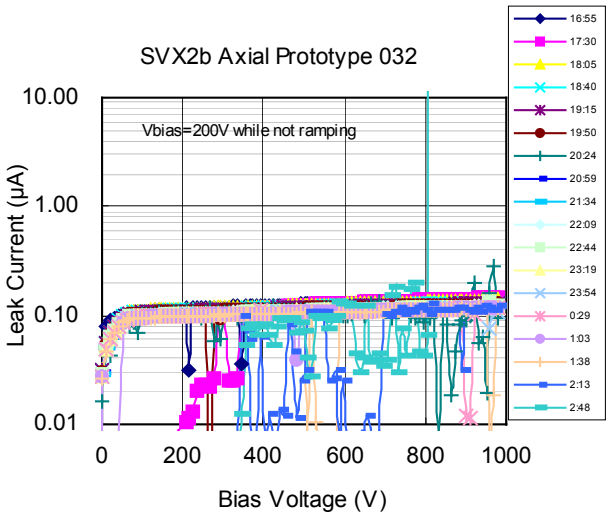

Fig. 2b Faulty I-V stability of sensor #032 (axial).

We measured the stability of I-V curves for sampled sensors including those which showed micro-discharges. The I-V measurement was repeated 20-30 times (10 times for some sensors). Between the I-V measurements, the sensors are biased to 200V and kept for 30 minutes. Figure 2a overlays I-V curves measured for a typical sensor, stereo #045. The curves are consistent and stable although the initial I-V tends to be somewhat different. This may be attributed to that the sensor surface condition is being stabilized in time between. Among the 6 axial sensors we measured, 5 sensors showed similar to the figure. One sensor (axial #032: see Fig. 2b) showed initially good I-V. The I-V curves became in chaos after 7hr and the sensor drew a large current at 800V after 10 hr. We investigated the cause with an IR camera and found a deep trace of discharge on the bias -ring. We suspect
that a discharge occurred between the bias-ring (which is DC connected to a p+ implant underneath) and the substrate probably due to some defect in the wafer. The I-V of this sensor has no recovered indicating existence of permanent junction breakdown.

For stereo sensors, we measured I-V stability for 10 sensors. Sensor #010 (see Fig. 2c), which

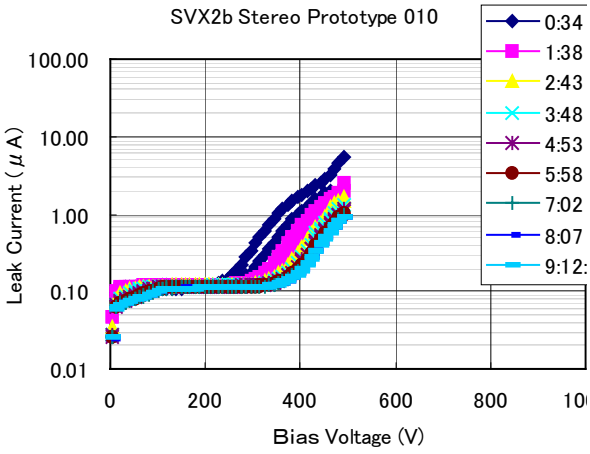

Fig. 2c I-V stability of sensor #010 (stereo).

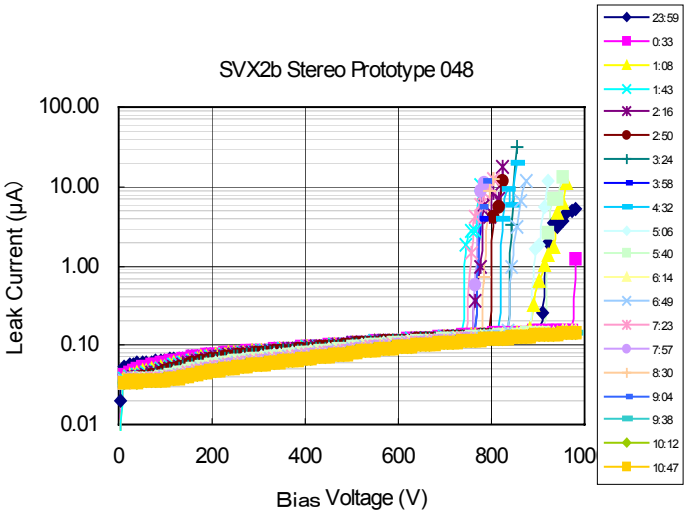

Fig. 2d I-V stability of sensor #048 (stereo).

showed micro-discharge in the initial I-V, improves the I-V curve gradually. The micro-discharge onset voltage of Sensor #048 (see Fig. 2d) was fluctuating around 800V. The I-V became flat to 1000V in the last three measurements. Note that the initial I-V is already better than the one shown in Fig. 1b because the sensor was biased for other test before this stability test was made. Other sensors showed stable I-V curves up to 1000V.

3.3 C-V curves

The C-V curves are measured for 19 axial and 53 stereo sensors at an LCR frequency of 400 Hz. We extract the full depletion voltage as the intercept of two straight lines in a C-$V^{-1/2}$ plot (see Fig. 3a). HPK measures C-V at a voltage step of 10V. The data is used to evaluate the "full depletion voltage", which is defined to be the lowest voltage where the increase of $1/C^2$ is found to be less than 2%. There is a tendency that HPK gives somewhat larger voltage, as can be seen in Fig. 3b. The distributions of Tsukuba data (axial and stereo separately) and of HPK are given in Fig. 3c. The spread of the distributions are similar, indicating that the full depletion voltages are extracted consistently apart from the absolute value. As a matter of fact, the value 2% is an arbitral choice so that no fitting is necessarily performed. For a choice of 4%, the agreement between the two should be improved. Three sensors have failed in the full depletion voltage specification, but all of them are more than 115V.

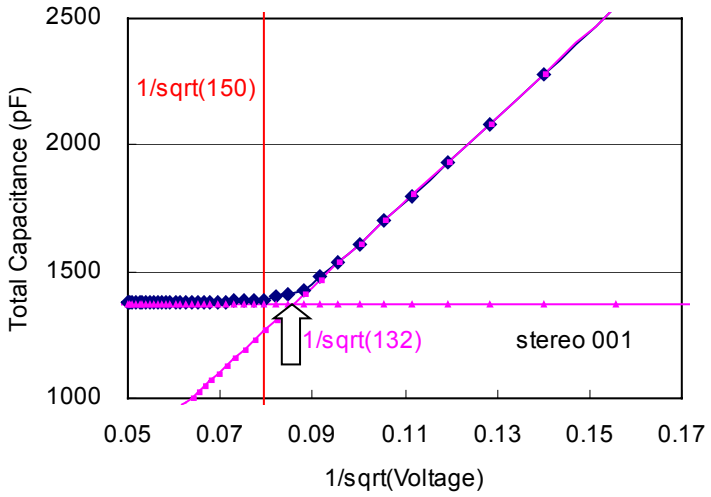

Fig. 3a C-V curve and evaluation of "the full depletion voltage". HPK determines (see text) it to be 150V, whereas we obtain 132V for this sensor, stereo #001.

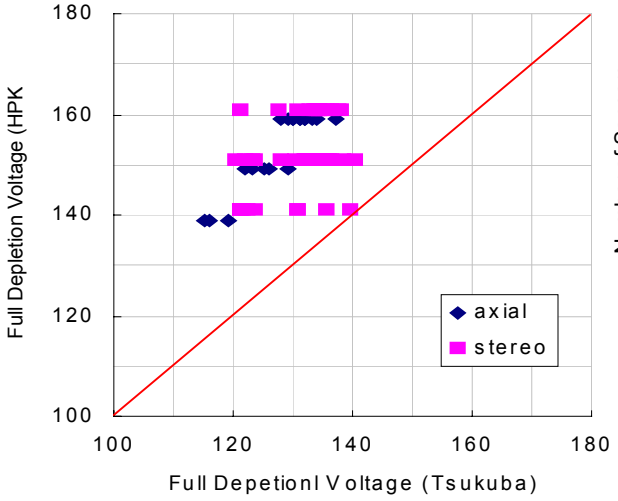

Fig. 3b Correlation of full depletion voltages defined by HPK and Tsukuba.

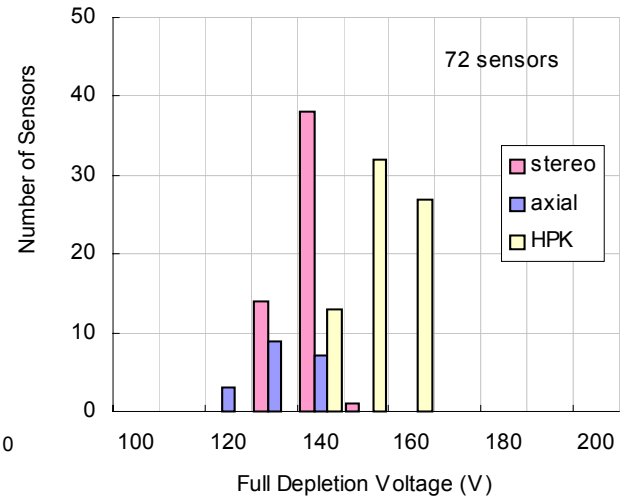

Fig. 3c Full depletion voltage distributions for axial and stereo sensors (Tsukuba) and for all (HPK).

3.4 AC scan

The strip integrity is intensively evaluated by AC scan where the measurement is performed in two steps. Firstly, capacitance and series resistance are measured by probing between the AC pad and bias-ring setting the LCR at Cs-Rs mode. Secondly, 100V is applied across for 1 second and then the leakage current through is measured. The capacitance represents the oxide coupling capacitance, and the resistance the sum of the bias resistance and implant electrode resistance. The latter contributes approximately 0.3-0.5 MΩ.

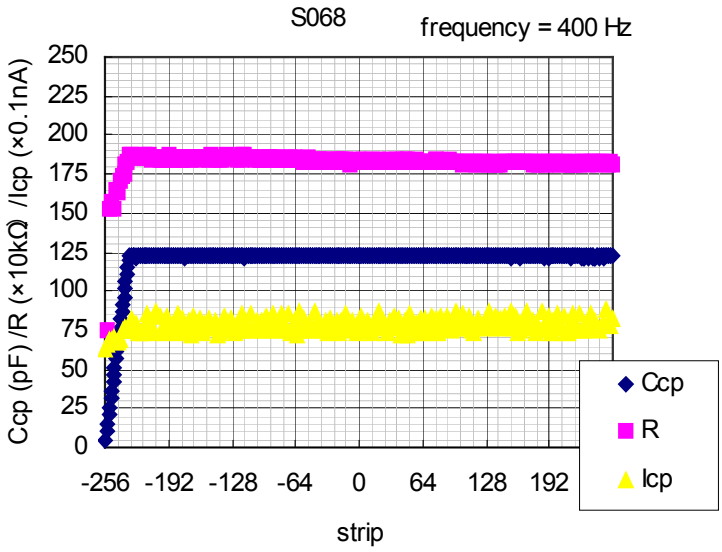

Fig. 4a Example of AC scan result (Stereo #068).

An example is shown in Fig. 4a, where the AC scan results are shown for stereo #068. Nominal values are about 120 pF (coupling capacitance), 1.85 MΩ (series resistance), and 7.5 nA (leakage) for strips with full length. As shown in the figure, coupling capacitance and R are smaller for shorter strips. Note that the 1st data point of R is small due to the frequency setting (1 kHz) is not at the optimum. Most part of the measured leakage is actually through relays used in the measurement system. The leakage through oxide layer is much smaller, and the protection resistors determine the leakage to ~9μA if the oxide is completely punch-through .

Some example results are shown in Fig.4b, where we found some defective strips. In total, AC scan is made for 18 axial sensors and 18 stereo sensors. The comparison of dead channels reported by HPK is described later. Among the defective strips, there are a couple of readout strips which showed irregular values and we found clear breaks in the implant strips. An example of such AC scans is given in Fig. 4c, where RD24 (-24 in the plot) has smaller R and Ccp values.

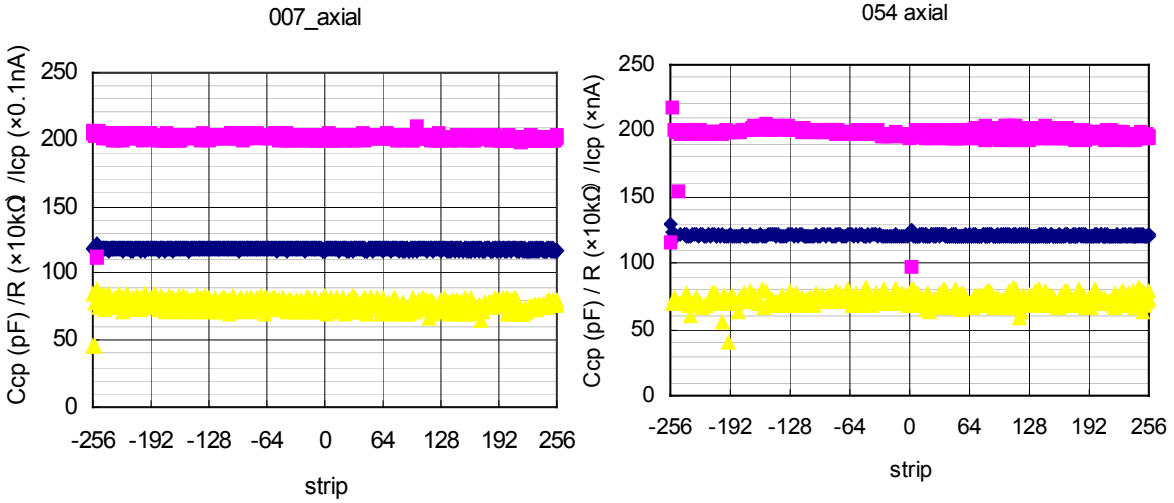

Fig. 4b AC scan result for (left) axial #007 and (right) axial #054

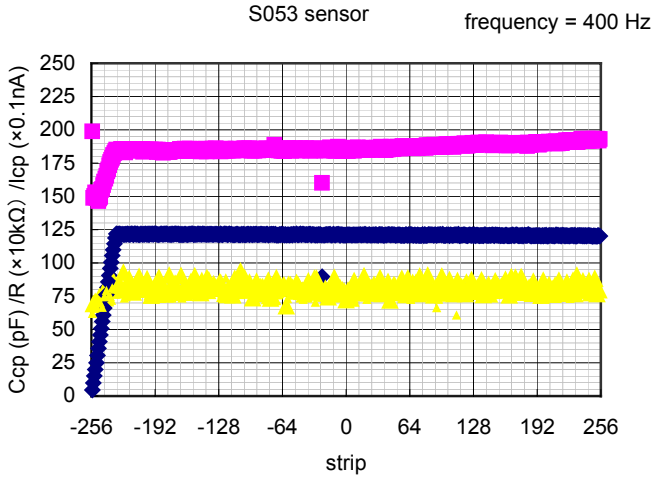

Fig. 4d AC scan result for stereo #053. One strip (-24) shows smaller R and Ccp values. This was not recognized by HPK, but a clear break was found in implant strip.

3.5 DC scan

The DC scan was made only for leaky sensors. An example result is given in Fig. 5, where the total leakage current evolution during the measurement is also plotted for stereo sensor #010. The bias is set to 400 V, above the micro-discharge onset voltage. The total leakage decreases as the measurement proceeds, as we have seen in I-V stability test. Since the total leakage current is about 0.1-0.2 μA for good sensors, the excess of this sensor is initially about 1 μA and finally 0.1 μA. The excess is totally explained by a single leaky strip, U225. This strip is classified as dead (Leaky) by HPK. Another leaky Sensor (stereo #048) has also single leaky intermediate strip, which is identified by HPK.

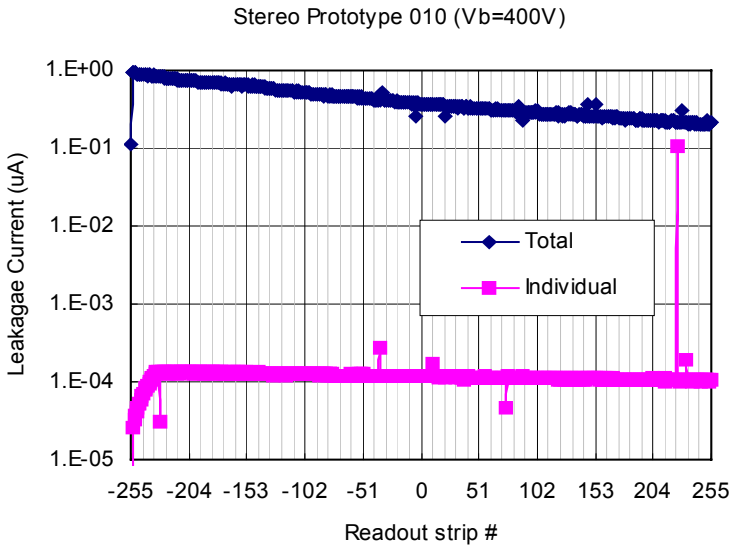

Fig. 5 DC scan (stereo #010) measured at 400V

3.6 Interstrip Resistance

The interstrip resistance is evaluated by measuring the increase/decrease in the strip leakage current when DC voltages ($\pm 1, \pm 0.5$ V) are applied to the intermediate strips at neighbor. The four resistance values so obtained are averaged to represent the interstrip resistance. Two examples are shown in Fig. 6. Although the characteristics are different for these sensors, the averages are 50-200 GΩ and no strip is smaller than 1 GΩ, which is our specification. Another sample (Axial 016) showed a distribution very similar to 026 Sensor. We suspect that 001, which was measured right after the delivery (i.e. production), is exceptional, and usual sensors should look like 026 Sensor after the surface charge is stabilized. Unfortunately 001 can not be re-measured since it is used for irradiation with neutrons.

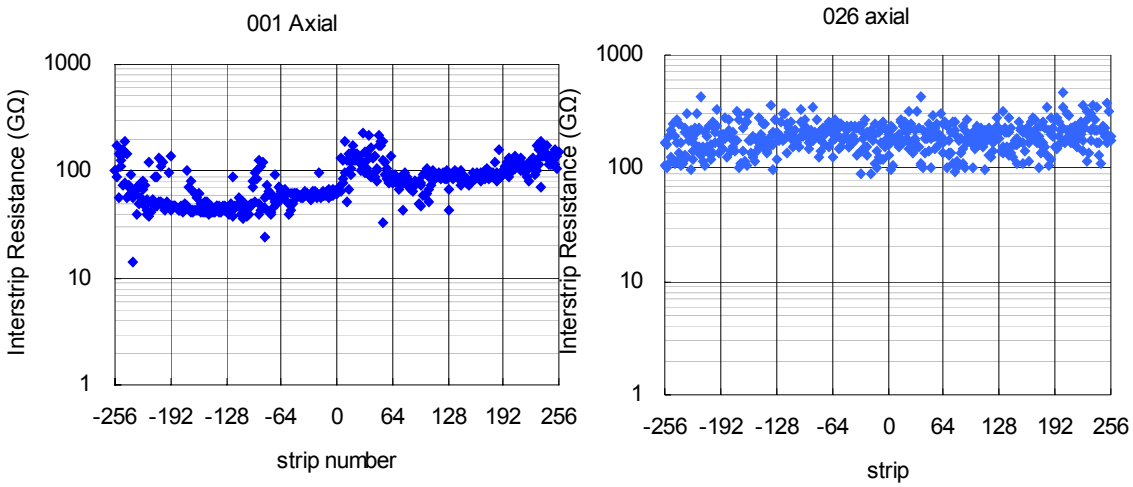

Fig. 6 Interstrip resistance of (left) 001 axial and (right) axial 026 Sensors.

3.7 Interstrip Capacitance

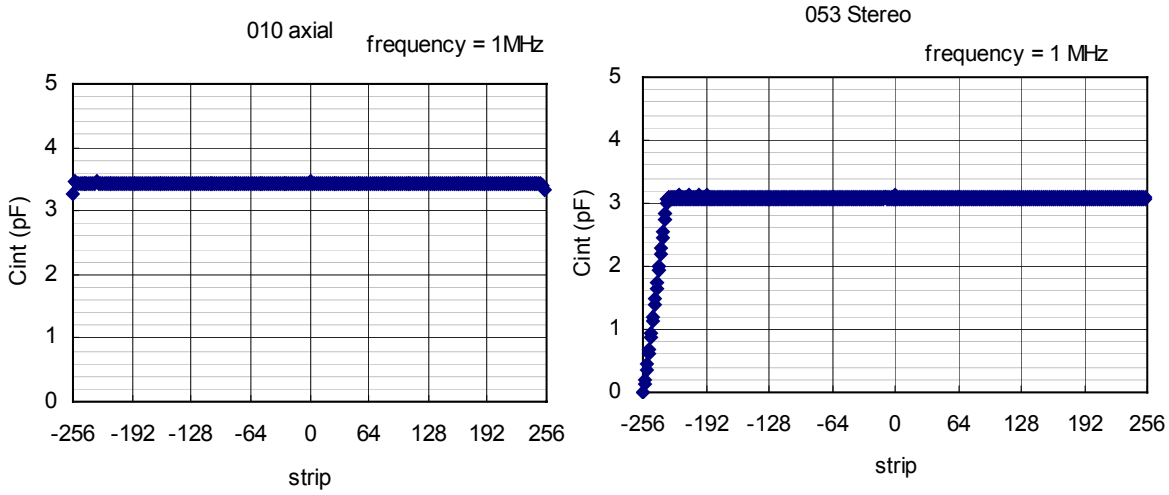

Fig. 7a Interstrip capacitance for (left) axial 010 Sensor and (right) Stereo 053 Sensor.

The interstrip capacitance is measured by probing neighboring (readout) AC pads with other strip at floating. The bias is set to 200 V and the LCR frequency at 1 MHz. The interstrip capacitance is uniform representing the strip length (See Fig 7a). Note that the absolute value difference of 0.3 pF should be the limit in the absolute calibration of our system.

We have measured the interstrip capacitance of in total 9 axial and 2 stereo sensors. Although most of the sensors have distributions quite similar to those in Fig. 7a, 1 axial and 1 stereo

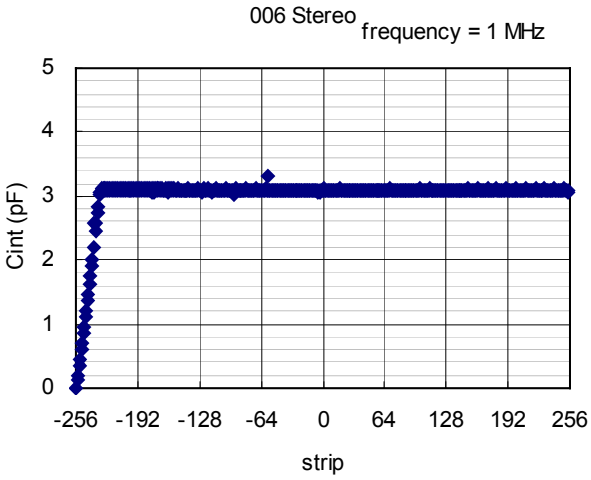

Fig. 7b Interstrip capacitance: Sensor 006 (Stereo) with an irregular value.

sensors showed irregular values, one pairs for each. An example is given in Fig. 7b. In fact the irregularity for this sensor did not present at the first measurement, but it appeared. In the ime between the probe scratched out the AC pad by mis-operation. Similar thing may have happened to other sensor, and we suspect these irregularities are created during the testing at Tsukuba. There is no other problem found for these strips by visual inspection under microscope.

3.8 Long-term stability test

The stability of leakage current is tested for in total eight sensors (4 axial and 4 stereo sensors) for a longer term. The bias voltage is kept at 500 V and the whole setup is placed in an environment chamber at 20°C. The leakage current data are taken typically once per day (the measurement is still on going). In addition to this, the durability of AC oxide is tested: 30 AC pads per sensor are wire bonded to an external voltage of +100V while the bias-ring is set to the ground level. It turns out the leakage current increases substantially when this external 100V is applied because of micro-discharge underneath the extended Al electrodes. Therefore, we decided to turn off this voltage for 1 hr prior to the leakage current measurement. The leakage current since Dec 4 when this decision was made is almost stable.

Out of eight sensors, one axial sensor (A23) showed breakdown at the AC oxide, indicating a creation of punch-through, on the 2nd day. Note again that axial sensors had been tested only at 100V prior. Other seven sensors are good so far.

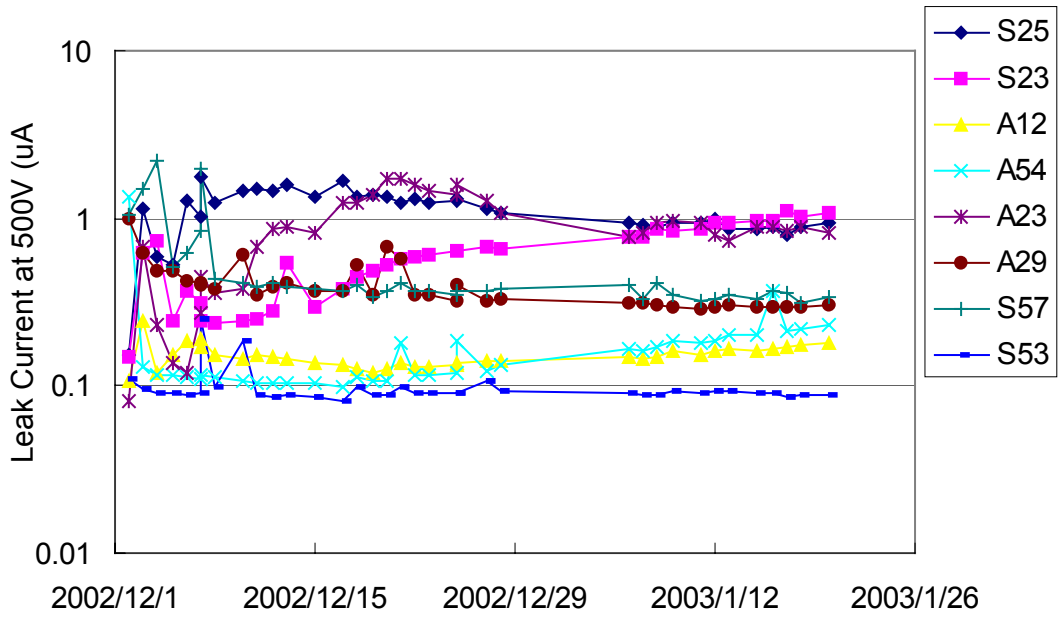

Fig. 8a Long-term stability test of leakage current. The temperature is 20°C and the bias is 500V. Note the change in the measurement procedure (see text) after 2002/12/05.

3.9 Visual Inspections

The delivered sensors have been visually inspected under a microscope. Also, faulty strips reported by HPK and found by our scan are inspected more carefully.

The axial sensors are in general clean and we did not recognize major flaws. As described in Section 2, the stereo sensors, on the contrary, showed visible problems. Figure 8a is a typical picture found for about 2/3 of Class B stereo sensors. Enlarged view shows that the scratches are on the very surface of Al traces. These scratches are created when the wafers were taken out manually from the process line, which is not expected to happen in the production. We checked if there is any correlation between faulty strips and the scratches, but there seems no correlation.

A yellow spot shown in Fig. 8b is found only for Stereo 010 sensor. Stereo 010 Sensor showed micro-discharge, but the contributing strip is not the one in this yellow spot.

From these observations, we conclude that these sensors are good in electrical performance. We classify them as Class B (do not use them, unless delivery becomes a major problem for completion of the project) .

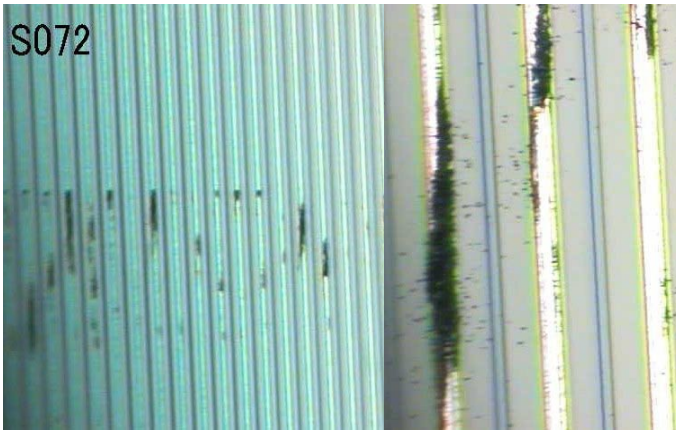

Fig. 8a Example of scratches observed for stereo sensors. (Right) Enlarged view.

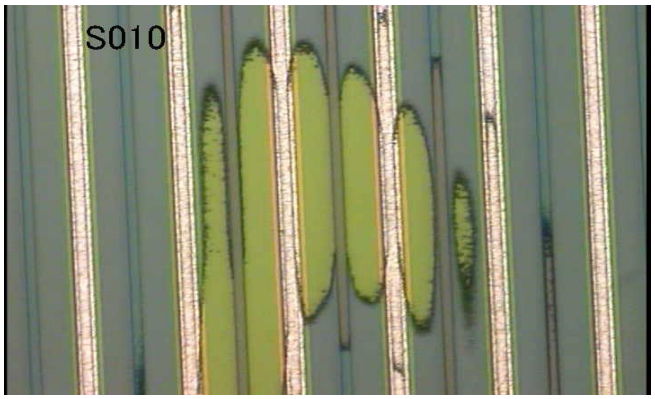

Fig. 8b Yellow spot found for Stereo 010 Sensor.

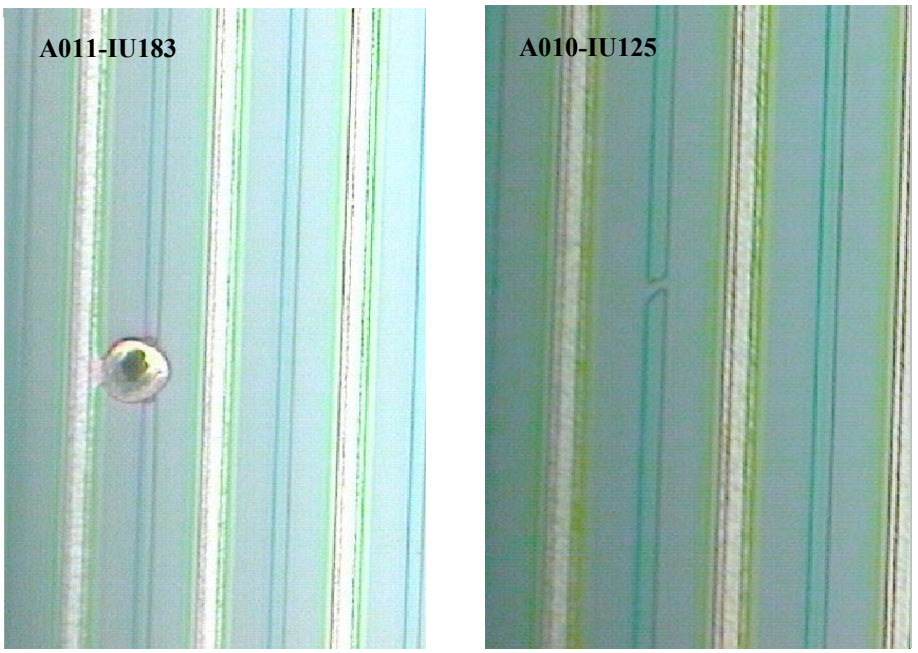

Fig. 8c Example of implant opens. (Left) Axial 011 Sensor and (Right) Axial 010 Sensor

Figure 8c shows examples of implant opens. Typical implant opens are similar to the one found for Axial 010 Sensor (intermediate strip U125).

4. Summary of the QA Measurements and Comparison with Manufacturer's Data

4.1 Axial Prototypes

Out of 60 delivered sensors, 20 sensors are retained in Tsukuba and 18 are studied in detail the characteristics described so far. Sensors with dead channels and worse I-V characteristics are preferentially retained in Tsukuba. (All the sensors shipped to Fermilab have no dead channels reported by HPK.) Table 2 summarizes the dead channels compared between HPK and Tsukuba measurements.

The reason for the dead is given in the parentheses. In red, we denote that we found new defects and the reason is understood: an open implant is recognized by microscope (implant open) or the oxide punch-through (large leak through oxide). If we can not identify the reason for new defects, they are in blue. The two strips (I-U244 and I-U241; "I" refers intermediate strip and "R" readout strip) of Sensor 10 have no obvious opens found, but the resistance measured between the DC pad and the biasing was large. The bias resistor is located other end for the intermediate strips and probably the joint between the DC pad and implant strip is not fine, which can not be identified by microscope. None of the leaky strips (Sensor 54) and bad isolation strips (Sensor 67) was identified at Tsukuba. It is quite possible that they disappear by keeping bias on for a while, as seen in 3.2 and as described in Section 5. Therefore, we fully understood the defects reported by HPK.

In total 12 punch-throughs are "created" by Tsukuba measurement. After discussion with HPK engineer, it turned out that HPK tested the punch-through by applying a voltage of 100 V for 1/6 sec. Since we apply 100V for 1 sec (or multiple of 1 sec if the measurement is repeated), it is not strange that some punch-throughs are created. HPK should have tested at 120 V, which is the specification and was actually the case for the stereo prototypes. We can ignore these disagreements since we did not see any punch-through for stereo sensors, as described later.

Table 2. Dead channels of axial prototypes compared between HPK and Tsukuba measurements. For disagreements, channels with clear defects are in red and others in blue.

sensor	HPK	Tsukuba
1		
2		
5		RU62 (Ccp=93pF, R=1.77MΩ,Implant open)
7		RD252 (R=1.1MΩ) RD251 (R=1.1MΩ) trace of small discharge
10	IU244 (Implant open)	IU244 (R=large)
	IU241 (Implant open)	IU241 (R=large)
	IU126 (Implant open)	IU126 (Implant open)
11	IU183 (Implant open)	IU183 (Implant open)
12		RU240 (Ccp=1.07nF, R=2.94MΩ, Icp=8.1uA)
16		
20		RD231 (167pF, 1.45MΩ, 6uA) RD217 (887pF, 2.63MΩ, 8uA)
21		
23		RD242 (252pF,3.7MΩ,8uA), RD241 (149pF,2.9MΩ, 8uA) RD240 (4860pF, 1.7MΩ, 8.3uA) RD200 (197pF, 3.7MΩ, 8uA) RD194 (155pF, 3.7MΩ, 8uA), RD116 (1920pF, 2.6MΩ, 8uA)
26		
53		
54	ID237, ID240 (Leaky strip) RD249, RD250 (Leaky strip)	RD256 (129pF, 1.15MΩ, 8.1uA)
		RD249 (120pF, 2.0MΩ, 1.5uA)
		RD248 (3291pF, 1.6MΩ, 8.3uA)
		RD244 (292pF, 3.7MΩ, 8.0uA)
56		
62		
64		
67	ID229, ID230, RD230 (Bad isolation)	RU136 (Ccp=80pF, R=1.6MΩ, implant open)

Sensors 5 and 67 have one implant open for each, which was detected at first by AC scan and then identified by microscope, whereas HPK could not detect it. A possible explanation is given in Section 4.3 after describing the summary for stereo sensors.

After all, two strips (Sensor 7, RD251 and RD 252) are new and not fully understood. This sensor (and some other sensors) is sent back to HPK to investigate the problem. According to HPK investigation, small discharge should have happened. The photograph taken by HPK is shown in Fig. 8d. The DC pads of these strips are colored and black discharge traces are visible bridging the two pads.

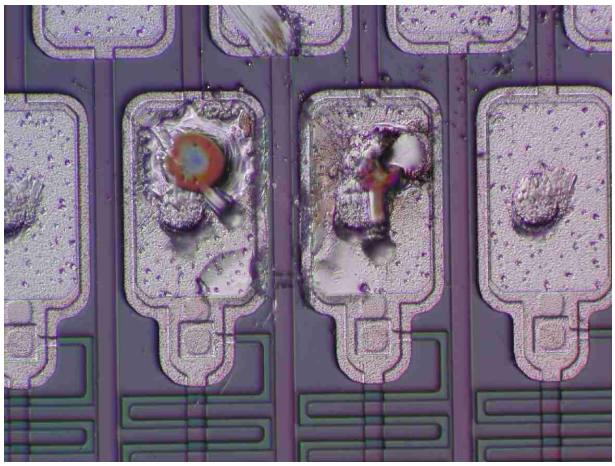

Fig. 8d Photograph around DC pads of RD251 and RD252. Two black traces are visible bridging the two DC pads. (Photo taken by HPK)

4.2 Stereo Prototypes

Out of 53 delivered sensors, 18 sensors are studied in detail on the strip integrity. The comparison is given in Table 3. All the defect strips reported by HPK are identified at Tsukuba. In addition, we found three identified implant opens for readout strips (Sensor 10, RU75; Sensor 23, RU2; Sensor 53, RD24), and one un-identified defective strip (Sensor 13, RD83). There is no punch-through created since HPK tested at 120V, as described in 4.1.

Table 3. Dead channels of stereo prototypes compared between HPK and Tsukuba measurements. For disagreements, channels with clear defects are in red and others in blue.

sensor	**HPK**	**Tsukuba**
6		
7		
10	RU225 (Leaky)	RU225 (leaky)
		RU75 (C=55,R=1.16; implant open)
23		RU2 (C=40,R=0.88; implant open)
24		
47	IU158 (Implant open)	IU158 (Implant open)
65	IU59 (Implant open)	IU59 (R=20M)
66	IU238 (Implant open)	IU238 (implant open)
68	IU21 (Implant open)	IU21 (implant open)
69		
13		RD83 (C=111, R=1.77)
46		
49	IU147 (Implant open)	IU147(R=large)
50		
53	ID7 (Implant open)	ID7 (implant open)
		RD24 (C=90,R=1.6, implant open)
57	ID62 (Implant open)	ID62 (implant open)
63	ID146 (Implant open)	ID146 (implant open)
25	ID230 (Implant open)	ID230 (implant open)

4.3 Implant Opens and Some Technical Difficulties

We have detected five implant opens that were not detected by HPK. These are all readout strips. A possible explanation is sketched in Fig. 9. HPK carries out two kinds of tests; DC and AC tests. In the AC test, HPK injects a step pulse on the AC pad and measures the transient signal shape to detect oxide punch-through (evaluate coupling capacitance) and Aluminum strip break/bridge. This procedure is reliable and has been used for many years. In the DC test, HPK applies a DC voltage between the DC pad and bias-ring, and measures the current. This is most sensitive for poly-silicon resistance but also can provide information for the implant open and strip isolation. Since the intermediate strip implant is connected to the bias resistor at far end, the measurement is sensitive to any break in the implant. On the contrary, the system is not sensitive for the readout strip since the implant is connected to the ground at the probing end. Since we do not request DC pads on other end to avoid openings where hybrids are glued, it is not possible to enhance the sensitivity for readout strips. HPK is expecting opens locating near end should also be detected for readout strips. The three opens detected by Tsukuba are located about 2 cm, 7cm and 8 cm from the probing end[1]. We have to conclude that the HPK measurement is barely sensitive for detecting readout implant opens.

There is no reason for the fraction of implant opens being different for intermediate and readout strips. HPK reports 13 opens for the intermediate while we identified three opens for the readout. Therefore it is probable that we are still missing some more readout implant opens. Also we should foresee to have some un-identified readout implant opens since it is not able to probe every strip for all the delivered sensors.

Similar difficulties exist for stereo sensors. In our design most of the short strips which are measured are not connected to the hybrid, but 12 or 19 strips not measured will be connected. The AC pads for these strips are located other end located under the hybrid, and are passivated. The nearby bias-ring is also passivated. Although we could open the passivation to test, but changing the set-up to measure for these extra strips only is a time consuming task, which HPK wants to avoid. It is a reasonable decision not to measure these short strips.

We therefore have to accept some un-identified defective short strips and implant opens to exist before connecting to the hybrid. It should be safe to say that if the number of identified defects is small, the number of un-identified defects should also be small. A good thing is that most of HPK sensors have zero defect! A possible scenario is to use preferentially the sensors with zero or a few defects, and other sensors are used for integrity test.

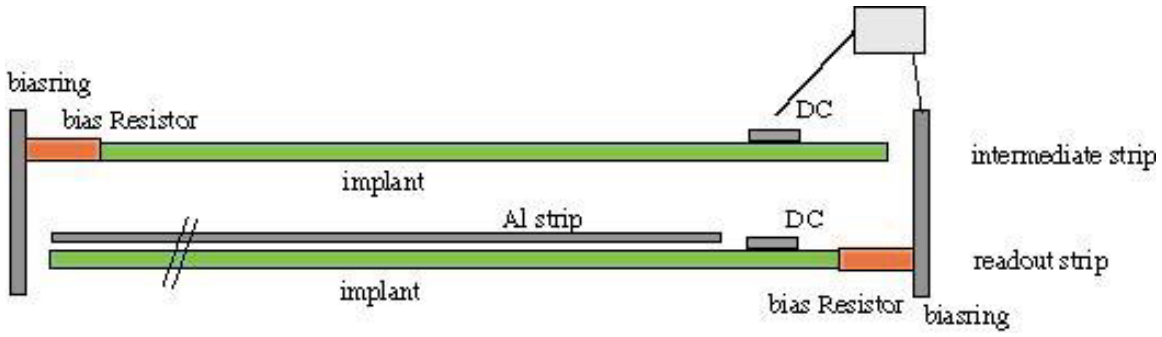

Fig. 9 Illustration of measurement configurations of readout and intermediate implant opens.

[1] HPK re-visited their data if there is any hint for these three strips and also re-measured some of the sensors with readout implant opens, but failed to identify the defects.